Northumbria Research Link

An Adaptive Charging Strategy of Lithium-ion Battery for Loss Reduction with Thermal Effect Consideration

Yujie Ding
a) Department of Mathematics, Physics and Electrical Engineering
Northumbria University
Newcastle, United Kingdom
b) School of Electrical Engineering
Southeast University
Nanjing, China
yujie2.ding@northumbria.ac.uk

Haimeng Wu
Department of Mathematics, Physics and Electrical Engineering
Northumbria University
Newcastle, United Kingdom
haimeng.wu@northumbria.ac.uk

Zhiwei Gao
Department of Mathematics, Physics and Electrical Engineering
Northumbria University
Newcastle, United Kingdom
zhiwei.gao@northumbria.ac.uk

Hailong Zhang
School of Electrical and Automation Engineering
Nanjing Normal University
Nanjing, China
61204@njnu.edu.cn

Abstract—With the increasing deployment of the electric vehicles, the study of advanced battery charging strategy has become of great significance to improve charging performance with reduced loss. This paper presents an optimized adaptive charging strategy for EV battery packs based on a developed system loss model. An electrical model integrated with thermal properties for the lithium-ion battery with cooling as well as a full loss model for the power converter have been included in this complete model. To reduce the overall loss of the charging system, the influence of temperature and varying internal resistance at different state of charge (*SOC*) have been considered to obtain an objective function. Moreover, an enhanced particle swarm optimization (*PSO*) algorithm is proposed and applied to speed up convergence time as well as enhance the precision of the solution. The results show that this proposed strategy can reduce the total loss by 4.01% and a 7.48% decrease of the charging time compared with the classical approach without applying this optimization.

Keywords—lithium-ion battery, charging strategy, loss minimization, particle swarm optimization

I. INTRODUCTION

In recent years, lithium-ion batteries have become main energy storage media in portable equipment, industrial electronics, aerospace and other fields because of their high energy density, low self-discharge rate, long cycle life, and minor pollution [1]. Due to market booming in electric vehicles (EVs), the demand on increasing the batteries' charging rate and efficiency has become a widespread concern [2, 3], which puts forward higher requirements on the charging strategy. Generally, an accurate system model and an advantageous charging strategy are critical to the performance of the battery, which should be the result of a comprehensive weighing between the charging time, energy loss, battery aging, and hardware cost.

Many studies have contributed to the models of the lithium-ion batteries as well as the power converters in the battery charging system to perform optimizations from different perspectives such as temperature rise and internal resistance with state of charge (SOC) [4-8]. From the standpoint of efficiency, the commonly used constant current (CC) charging, constant voltage (CV) charging, constant power (CP) charging, and an optimized charging considering temperature rise have been compared and discussed in [9], whereas the study assumes that all the internal resistances of the lithium-ion batteries are not related to the state of charge (SOC) which cannot reflect the real relationship of the parameters in the battery. In [10], the fluctuation of battery internal resistance with SOC is considered, however, the change of internal resistance with temperature is ignored. To take the thermal issues into account, a constant-temperature constant-voltage charging technique is proposed that aims to prevent battery ageing process caused by overheating, whereas the research neglects the damage to the battery caused by the high charging current in the low state of charge (SOC) region [11].

Many optimization methods have been applied to solve the optimal charging problems, for instance, genetic algorithm [12], dynamic programming [9], Taguchi method [13], etc. However, limited by their search mechanism, these methods are not the most efficient algorithms for solving problems in continuous solution spaces. Moreover, the traditional particle swarm optimization (PSO) algorithm also shows unsatisfactory results on problems with a vast solution space [14].

Therefore, this paper proposes an optimized adaptive charging strategy for EV battery packs, which aims to further enhance the charging performance by employing a more comprehensive system loss model. Specifically, to analyze the loss of the system close to the real-world settings, an electrical model including thermal properties for the lithium-ion battery with cooling is developed. As a result, a system loss model with the optimized objective function is obtained to make a tradeoff between the battery internal loss and the loss of power conversion stage. Furthermore, an enhanced PSO algorithm with a large-scale optimization is proposed to achieve fast solving of the optimal solution as well as to enhance precision of the results.

II. SYSTEM MODELLING

The battery charging system is presented in Fig. 1, which is composed of a dual active bridge (DAB) DC-DC converter and an EV battery pack with built-in cooling device.
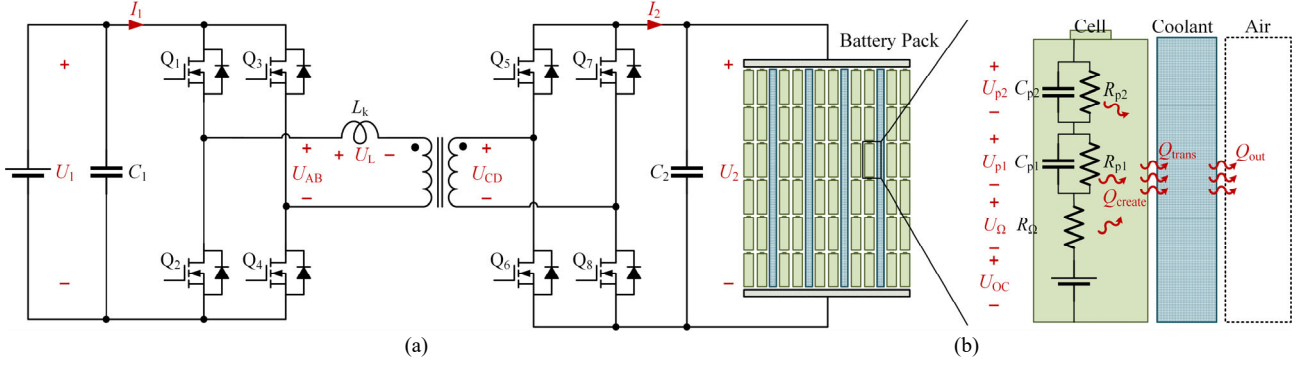
Fig. 1. Schematic of the battery charging system. (a) power converter. (b) EV battery model.

A. Battery electrothermal model

The external electrical characteristics of the lithium-ion battery can be modelled by a universal equivalent model [15]. Typically, a second-order Thevenin equivalent model is shown in Fig. 1(b), which is composed of an open-circuit voltage (OCV) source, an ohmic resistance, and a resistance-capacitance network that reflects the polarization phenomenon. The full battery electrothermal model can be expressed in (1) to (5). Equation (1) and (2) draw the dynamic characteristics of the battery, and (3), (4), and (5) describe the battery's voltage, internal loss, and SOC during the charging process, respectively.

$$C_{p1}\frac{dU_{p1}}{dt}+\frac{U_{p1}}{R_{p1}}=i_{tot} \tag{1}$$

$$C_{p2}\frac{dU_{p2}}{dt}+\frac{U_{p2}}{R_{p2}}=i_{tot} \tag{2}$$

$$U_{tml}-U_{p1}-U_{p2}-U_{\Omega}=U_{OC} \tag{3}$$

$$p_{loss}=i_{tot}^2 R_{\Omega}+\frac{U_{p1}^2}{R_{p1}}+\frac{U_{p2}^2}{R_{p2}} \tag{4}$$

$$SOC=\frac{1}{Ah}\int_0^t i_{tot}dt+SOC(0) \tag{5}$$

In the expressions above, U_{tml} is the terminal voltage of the battery, U_{OC} is the battery internal potential OCV, U_{Ω} is the ohmic internal potential which is proportional to the charge and discharge current, and U_p represents the polarization potential that has a gradual decay process after the removal of charge and discharge current; R_{Ω}, R_{p1}, C_{p1}, R_{p2}, and C_{p2} are the equivalent parameters of the battery; i_{tot}, p_{loss}, and Ah denote the total charge or discharge current, the total power loss on the internal resistance of the battery, and the capacity of the battery, respectively.

The time domain expression of the polarization voltage is suitable for both RC pairs that can be obtained by solving (1), as is shown in (6). This equation will be used in the simulation to mimic the dynamic characteristics of the battery.

$$U_p(t)=e^{-\frac{1}{R_p C_p}(t-t_0)}U_p(t_0)+\frac{1}{C_p}e^{-\frac{1}{R_p C_p}t}\int_{t_0}^t e^{\frac{1}{R_p C_p}\tau}i(\tau)d\tau \tag{6}$$

The liquid cooling system is widely applied in EVs, which should also be taken into account in the battery charging process. According to the heat transfer theory, the heat conduction between the battery and the environment via the coolant is modelled in this study. The heat generation can be expressed as (7), which is caused by the battery internal resistance and the rise of the internal voltage with temperature. The heat transfer can be expressed as (8) and (9), which shows a close relationship between the amount of heat exchange and the thermal conductivity as well as the area of the heat exchange interface.

$$Q_{create}=p_{loss}T_s+\frac{dU_{OC}}{dT}T_{bat}i_{tot}T_s \tag{7}$$

$$Q_{trans}=h_{bat}A_{bat}(T_{bat}-T_{cool})T_s \tag{8}$$

$$Q_{out}=h_{cool}A_{cool}(T_{cool}-T_{amb})T_s \tag{9}$$

In the equations above, Q_{create}, Q_{trans}, and Q_{out} are the heat generated by the battery, the heat transferred from the battery to the coolant, and the heat transferred from the coolant to the ambient; T_{bat}, T_{cool}, and T_{amb} are the temperatures of the battery, the coolant, and the ambient; h_{bat} and h_{cool} are the convection coefficient of the battery and the coolant; A_{bat} and A_{cool} are the thermal convection area of the battery and the coolant; T_s is the sample time.

The temperature can be calculated by (10) and (11) in accordance to the temperature rise characteristics of electrolyte and coolant.

$$Q_{create}-Q_{trans}=m_{bat}c_{bat}\Delta T_{bat} \tag{10}$$

$$Q_{trans}-Q_{amb}=m_{cool}c_{cool}\Delta T_{cool} \tag{11}$$

In the expressions above, m_{bat} and m_{cool} refer to the mass of the battery and the coolant respectively; c_{bat} and c_{cool} refer to the specific heat coefficients.

B. Charger loss model

The major components that cause the loss of the converter include MOSFETs, a high-frequency transformer, a resonant inductor, the wire resistance, and diodes due to the backward power flow [16].

The loss of MOSFET includes the switching loss, conduction loss, cut-off loss, and driver loss. Among them, switching loss is related to the state of the power switch (hard switching or soft switching), which can be determined by (12)

and (13) [17]. The power switches on the power supply side and the battery side are operated in the soft-switching state under the phase-shift control if they meet (12) and (13), respectively.

$$2D_{\varphi}+K-1>0 \quad (12)$$

$$K(1-2D_{\varphi})-1<0 \quad (13)$$

where K is the actual voltage ratio of the transformer, and D_{φ} is the phase shift. Then, the switching losses of hard switching and soft switching can be calculated according to (14) and (15) respectively. And the conduction loss can be obtained using (16)

$$P_{\mathrm{MOS, sw}} = \frac{1}{2}V_{\mathrm{DS}}I_{\mathrm{D}}t_{\mathrm{off\ to\ on}}f_{\mathrm{s}} + \frac{1}{2}V_{\mathrm{DS}}I_{\mathrm{D}}t_{\mathrm{on\ to\ off}}f_{\mathrm{s}} \quad (14)$$

$$P_{\mathrm{MOS, sw}} = \frac{1}{6}V_{\mathrm{DS}}I_{\mathrm{D}}t_{\mathrm{on\ to\ off}}f_{\mathrm{s}} + \frac{1}{3}I_{\mathrm{D}}^2 R_{\mathrm{on}}t_{\mathrm{on\ to\ off}}f_{\mathrm{s}} \quad (15)$$

$$P_{\mathrm{MOS, on}} = I_{\mathrm{D}}^2 R_{\mathrm{on}}t_{\mathrm{on}}f_{\mathrm{s}} \quad (16)$$

In the expressions above, V_{DS}, I_{D}, and R_{on} refer to the drain to source voltage when the power switch is off, the drain current when the power switch is on, and the conductive drain-to-source resistance; $t_{\mathrm{off\ to\ on}}$, $t_{\mathrm{on\ to\ off}}$, t_{on}, and f_{s} denote the total turn-on time, total turn-off time, conduction time, and the switching frequency. The cut-off loss and the driver loss are ignored in this paper.

The loss of the high frequency transformer mainly includes the copper winding loss, iron hysteresis loss, and iron eddy current loss, which can be calculated separately according to (17), (18), and (19) [18].

$$P_{\mathrm{TRANS, Cu}} = I^2 \kappa_{\mathrm{AC}}R_{\mathrm{DC}} \quad (17)$$

where I, κ_{AC}, and R_{DC} are the rms value of the winding current, the AC resistivity coefficient due to the skin effect, and the winding DC resistance.

$$P_{\mathrm{TRANS, h}} = K_{\mathrm{h}}f_{\mathrm{s}}^{\beta}B_{\mathrm{m}}^{\alpha}V_{\mathrm{core}} \quad (18)$$

$$P_{\mathrm{TRANS, e}} = \frac{1}{6\rho_{\mathrm{core}}}(\pi\gamma_{\mathrm{core}}f_{\mathrm{s}}B_{\mathrm{m}})^2 \quad (19)$$

where K_{h}, α, and β are the parameters from the experiment; V_{core}, ρ_{core}, and γ_{core} denotes the volume, the resistivity, and the density of the iron core; f_{s} refers to the switching frequency, and B_{m} refers to the maximum magnetic induction intensity.

The losses of resonant inductance, diode and wire resistance are similar to the aforementioned loss calculations, which are not detailed in this paper.

C. System model

The system model with thermal effect is presented in Fig. 2, which includes the battery's electrical characteristics, heat and power converter losses. In this model, to link up with the PSO algorithm, the refined simulation interface realizes the conversion of low time-density current commands to step-level dense current signals. Other models are constructed as illustrated above. In the simulation, the real-time battery voltage and loss is calculated through the electrical proportion of the battery model, and the corresponding parameters are transmitted to the thermal model of the battery to calculate the amount of the heat transfer and temperature. The temperature is used in the next iteration to determine the parameters of the battery electrothermal model.

The fluctuation of the total internal resistance with SOC and cell temperature provides the opportunity for adaptive optimization of the whole charging process. This paper focuses on optimizing the loss of the CC charging because of its dominance in charging time and loss in most of the charging profiles. Within the same charging time, the CC stage can be subdivided into many small CC segments (the number is set to M) to form an adaptive variable current charging. The goal is to minimize the charging loss of the whole charging system, and the constraints of the battery and the converter need to be satisfied. Therefore, the optimized objective function can be written as (20). The compromise of optimization target between the battery internal loss and power charger loss can be determined by adjusting the parameters α_1 and α_2 in the equation.

$$
\begin{aligned}
f(x) &= \alpha_1 Q_{\mathrm{bat}} + \alpha_2 Q_{\mathrm{cvt}} \\
\mathrm{s.t.}\ 0 &< i_{\mathrm{tot}} < I_{\mathrm{max}} \\
U_{\mathrm{min}} &< U_{\mathrm{bat}} < U_{\mathrm{max}} \\
P_{\mathrm{min}} &< P_{\mathrm{cha}} < P_{\mathrm{max}} \\
0 &< \sum_{k=1}^{M}\frac{C_{\mathrm{cha}}}{Mi_{\mathrm{tot}}[k]} \le \frac{C_{\mathrm{cha}}}{I_{\mathrm{CC}}}
\end{aligned} \quad (20)
$$

This function is not differentiable and requires numerical iteration in the calculation process. Hence, a PSO algorithm is introduced and developed to achieve an optimized charging process to reduce the loss, which is shown in the following section.
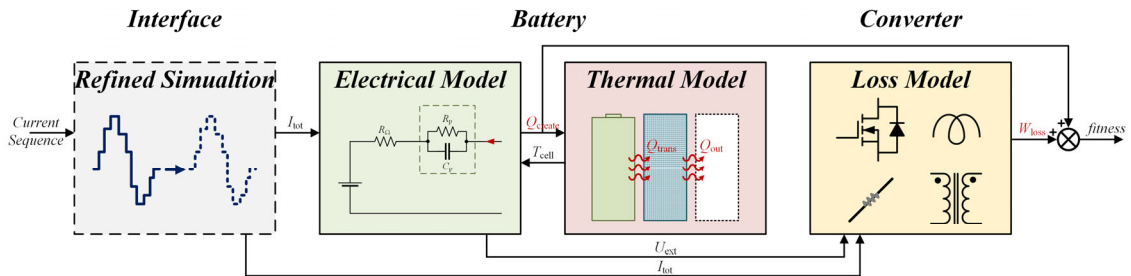

Fig. 2. System loss model with thermal effect

III. Optimized Charging Strategy

A. Enhanced PSO algorithm

1) Operation principles

The PSO algorithm iteratively obtain the optimal solution utilizing the historical optimal value of the group and the individuals. The flowchart of this iteration-driven algorithm is shown as Fig. 3. The collective cooperation between the particles enables the group to traverse most of the solution space and achieve the optimal goal with convergence. During the iterations, each particle records its historic optimal location (which is called as individual optimal), track the group's optimal location (which is called as group optimal), and update its velocity and position using (21) and (22) as follows, which is for particle i during the k th iteration.

$$v_i[k+1] = wv_i[k] + c_1 r_1 (x_{\text{iopt}i}[k] - x_i[k]) + c_2 r_2 (x_{\text{gopt}i}[k] - x_i[k]) \tag{21}$$

$$x_i[k+1] = x_i[k] + v_i[k+1] \tag{22}$$

In the expressions above, c_1 and c_2 are acceleration factors, w is the inertia weight which is normally in the range of [0.9, 1.2], and r_1 and r_2 are random numbers distributed in [0,1].

2) Enhancements

a) Reinitialization

As the iteration progresses, all particles will gather to the global optimal position, which results in a large quantity of calculations with little contribution to the search of the global optimal solution. In particular, the vast solution space of this problem puts forward higher requirements on the global optimization ability of the algorithm. The number of solutions reaches 10^19 even if the entire CC stage is only divided into 10 sub CC charging stages and only integer solutions are considered. By reinitializing a proportion of particles close to the global optimal location, the number of initial particles is equivalently increased and more paths are searched along,
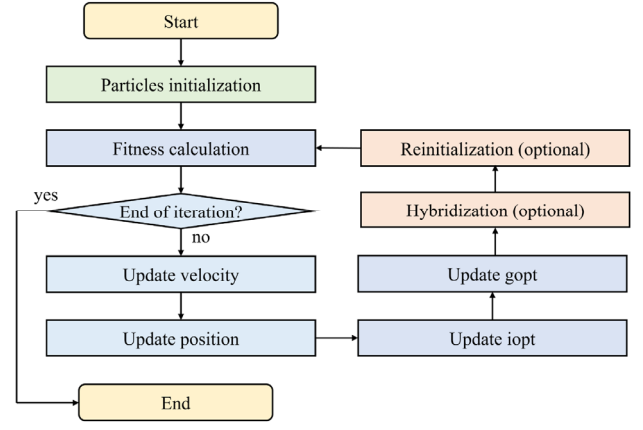

Fig. 3. Flowchart of the enhanced PSO algorithm

thereby significantly enlarging the probability of obtaining the global optimal solution. Reinitialization can be expressed as follows.

$$x = \text{randp}(I_{\min}, I_{\max}) \quad \forall \{x \| \|x\|_2 < \varepsilon \cap rand < 0.3\} \tag{23}$$

where $\text{randp}(a,b)$ is the initialization function, and $rand$ is a random number.

b) Hybridization

During the iterations, it is noticed that although the fitness of the particles can drop rapidly within 10 iterations, there is still a high probability of noise in the current solution waveform caused by random initialization. Given that it is essentially identical in this problem on the physical implication of each dimension of each particle, hybridization can be implemented by swapping the elements of the particles with best fitness. The hybridized particles are within a reasonable range and tend to aggregate because the hybridization is only performed on the particles with the best fitness, thus accelerating the approach to the global optimum. The criterion for hybridization is shown as (24). The fitness of each particle equals to the descendent ratio of the particle's
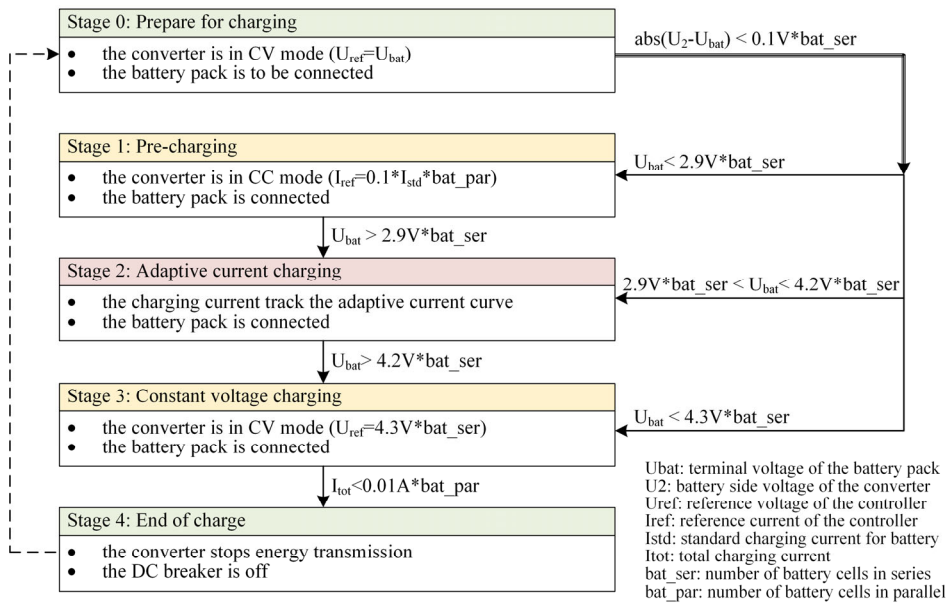

Fig. 4. Scheme of the PC-AC-CV charging strategy

objective function value compared with the objective function value of CC charging.

$$x = \text{swap}(x_i(k), x_j(k))$$
$$\forall \{x \| \text{ } fitness(x) - fitness(x_{\text{gopt}}) \| < \varepsilon \cap rand < 0.3\} \quad (24)$$

B. Charging Strategy

The full scheme of the proposed adaptive charging strategy is shown as Fig. 4, which consists of a pre-charging stage, an adaptive current stage, and a constant voltage stage (PC-AC-CV). In this figure, U_{bat}, U_2, and U_{ref} refer to the terminal voltage of the battery pack, the battery side voltage of the power converter, and the variable reference voltage of the controller; I_{tot}, I_{ref}, and I_{std} refer to the total charging current, the variable reference current of the controller, and the standard acceptable charging current of the battery; bat_ser and bat_par refer to the numbers of the battery cells in series and in parallel, respectively.

This control strategy has luring potential benefits in practice because of its simplicity and reliability. With regard to the second charging stage, the traditional CC charging is substituted with the adaptive current charging by utilizing the proposed enhanced PSO algorithm on the optimization of the battery charging system model. Due to its dominance in charging time and loss, the optimization of CC charging could bring considerable improvements to the entire charging process. For battery safety concerns, it is not recommendable to optimize the charging current in the entire SOC range since the battery can only bear with current within a designed range, especially in the low and high SOC regions. The PC stage applies a small charging current to smoothly rise the battery internal potential OCV, and the CV stage decays the charging current gradually to fully charge the battery while inhibiting voltage overshoot.

IV. SIMULATION EVALUATION

A. Simulation setup

The battery charging system consists of a 25 kW DAB DC-DC converter and a 15 kWh battery pack with 1225 NCR18650B cells. The parameters are shown in TABLE 1. Fig. 5 shows the battery's internal voltage, internal resistance, and internal capacitance at different SOC and temperature, which are obtained by hybrid pulse power characteristic (HPPC) test. It can be noticed that the internal resistance

TABLE I.   PARAMETERS OF THE BATTERY CHARGING SYSTEM

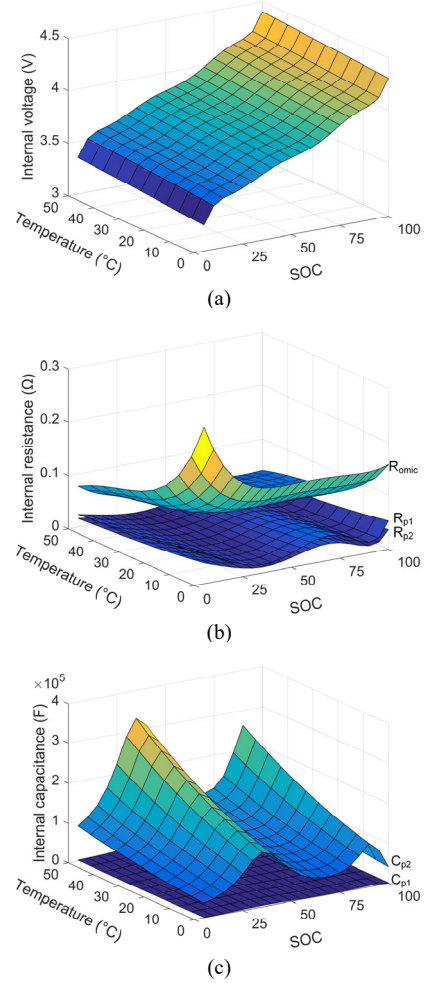| Parameters	Value
Battery prototype	NCR18605B (3.6 V, 3350 mAh)
Number of batteries in series	35
Number of batteries in parallel	35
Initial SOC	10%
Supply side voltage of the converter	200 V
Battery side voltage of the converter	150 V
Rated power of the converter	25 kW
Leakage inductance	10 uH

(a)

(b)

(c)

Fig. 5.   Parameters of the NCR18650B with SOC and temperature. (a) battery internal voltage. (b) internal resistance. (c) internal capacitance.
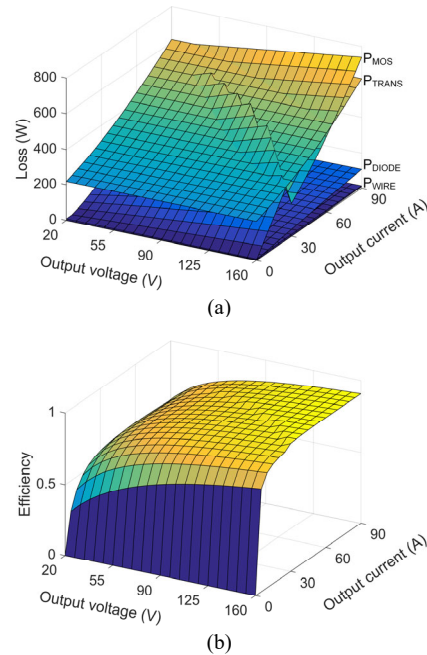
(a)

(b)

Fig. 6.   Loss model of the battery charger. (a) component loss. (b) efficiency map of the power converter.

fluctuates with the SOC, and that the internal resistance decreases with the increase of temperature. As an illustration of the converter loss model, the components' losses and the efficiency of the whole charger are shown in Fig. 6. The power converter shows a higher efficiency in heavier load region because of soft switching operation.

B. Effectiveness of the enhanced PSO algorithm

To investigate the charging optimization in this paper, the PSO algorithm is operated under different parameters, i.e., 9000 particles without enhancement, 3000 particles without enhancement, 3000 particles with one and both of the enhancement measures, as shown in Fig. 7. Here, the number of particles is the result of a compromise between the calculation complexity and the convergence of the solution, because the time of the solution procedure will increase with a higher accuracy as the number of particles increases. According to Fig. 7, it is evident that the adaptability of the PSO algorithm with 9000 particles decreases the fastest, while the optimization result of the PSO algorithm with 3000 particles is not satisfactory. Both reinitialization and hybridization can significantly speed up the convergence of the fitness (a comparison between the particles based on the improvements of the objective loss function), and 3000 particles with hybridization even obtains a better fitness than 9000 particles, which verifies the effectiveness of the proposed strategy. Since behavior of reinitialization and hybridization may differ on different problems, the combination of the two enhancements improves the robustness of the algorithm.
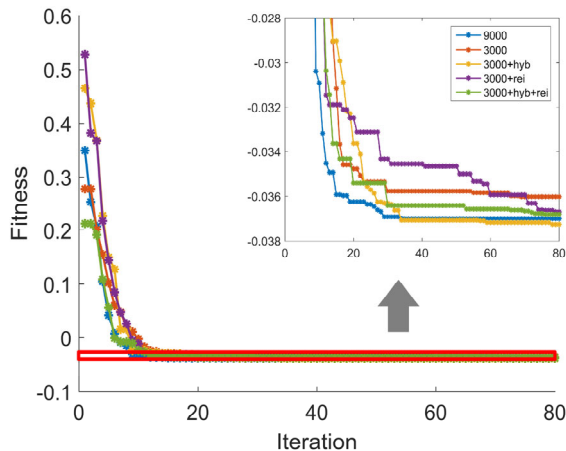

Fig. 7. Convergence of the enhanced PSO algorithm

C. Analysis of the proposed charging strategy

The optimized results for variable current charging compared with CC charging is analyzed as follows. The adaptive charging current is optimized into three scenarios: the optimization of the battery internal loss with the thermal effect, the optimization of the converter loss, and the optimization of the entire charging system. Taking CC charging at 0.5 charging rate as a comparison, the results are shown in TABLE 2. When the battery internal resistance loss is optimized, the battery internal loss is reduced by 0.51%, but the total loss is increased by 1.78% since the loss of the converter goes up by 3.50%. Similarly, 12.86% of the converter loss is declined when minimized, but the battery internal loss is excessively increased by 11.97%, for which the total loss is still not optimal. Only when the loss is optimized from the systematic perspective, a best solution can be

obtained (3.16% total loss reduction), which reveals the significance of model accuracy and comprehensiveness to the optimization results.

Regarding the proposed PC-AC-CV charging strategy, the complete charging waveform is shown in Fig. 8 compared with the CC-CV charging method. The adaptive charging current is appropriately lifted after the trade-off between battery internal loss and the power converter loss. In the zoomed-in subplot, the smoothed charging current fluctuates in the opposite direction compared with the internal resistance curve of the battery, which reduces the battery internal loss. The result shows that the loss of the entire charging process is reduced by 4.01%, and also shows an 8.5-minute decrease of the total charging time, which verifies the performance of the adaptive charging strategy

TABLE I. RESULTS OF DIFFERENT TARGETS

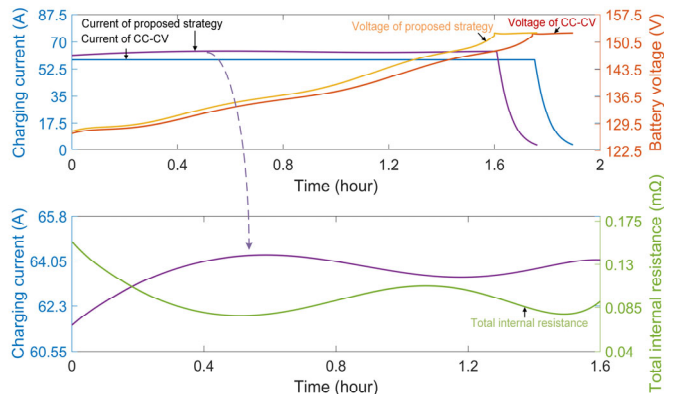| Charging strategy	Energy Loss (Wh)		
	Converter	*Battery pack*	*Total*
CC-CV	770.79[a]	579.34	1350.13
Battery internal loss minimized	797.79	576.40	1374.20
Converter loss minimized	671.68	648.67	1320.35
System overall loss minimized	684.29	623.17	1307.46

Fig. 8. Comparison of the proposed charging strategy and CC-CV method

V. CONCLUSION

An optimized adaptive charging strategy for EV battery packs is proposed in this paper based on a developed system loss model. This full model includes the electrothermal properties of the lithium-ion EV battery pack and an accurate loss estimation model for the power converter. Moreover, the enhanced particle swarm optimization (PSO) algorithm with reinitialization and hybridization is proposed to achieve an optimal charging process that can solve the large-scale non-differentiable issue effectively. The simulation verifies the effectiveness of the proposed strategy, which achieves a 4.01% reduction of the total loss with a 7.48% decrease of the charging time.

REFERENCES

[1] J. Jiang, C. Zhang, J. Wen, W. Zhang, and S. M. Sharkh, "An optimal charging method for li-ion batteries using a fuzzy-control approach based on polarization properties," IEEE Trans. Veh. Technol. vol. 62, pp. 3000-3009, May 2013.

[2] J. Ronald, "Electric vehicles (ev)," ed: SAE, 2002, pp. 1-1.

[3] F. Naseri, E. Farjah, and T. Ghanbari, "An efficient regenerative braking system based on battery/supercapacitor for electric, hybrid, and plug-in hybrid electric vehicles with bldc motor," IEEE Trans. Veh. Technol. Iran, vol. 66, pp. 3724-3738, May 2017.

[4] C. Zhang, K. Li, J. Deng, and S. Song, "Improved realtime state-of-charge estimation of lifepo4 battery based on a novel thermoelectric model," IEEE Trans. Ind. Electron. vol. 64, pp. 654-663, September 2016.

[5] H. Zhan, H. Wu, M. Muhammad, S. Lambert, and V. Pickert, "Combining electric vehicle battery charging and battery cell equalisation in one circuit," IET Electr. Syst. Transp. pp. 1-14,

[6] H. Wu, V. Pickert, S. Lambert, P. Allanf, X. Deng, and H. Zhan, "A ripple reduction method for a two stages battery charger with multi-winding transformer using notch filter," 2017 IEEE 12th International Conference on Power Electronics and Drive Systems. pp. 101-106, December 2017.

[7] S. Q. Zhu, C. Hu, Y. Xu, Y. Jin, and J. L. Shui, "Performance improvement of lithium -ion battery by pulse current," J. Energy Chem. China, vol. 46, pp. 208-214, July 2020.

[8] H. Wu, V. Pickert, X. Deng, D. Giaouris, W. Li, and X. He, "Polynomial curve slope compensation for peak-current-mode-controlled power converters," IEEE Trans. Ind. Electron. vol. 66, pp. 470-481, April 2018.

[9] Y. Parvini, A. Vahidi, and S. A. Fayazi, "Heuristic versus optimal charging of supercapacitors, lithium-ion, and lead-acid batteries: An efficiency point of view," IEEE Trans. Control Syst. Technol. vol. 26, pp. 167-180, March 2017.

[10] Z. Chen, B. Xia, C. C. Mi, and R. Xiong, "Loss-minimization-based charging strategy for lithium-ion battery," IEEE Trans. Ind. Appl. vol. 51, pp. 4121-4129, March 2015.

[11] S. Wang and Y. Liu, "A pso-based fuzzy-controlled searching for the optimal charge pattern of li-ion batteries," IEEE Trans. Ind. Electron. vol. 62, pp. 2983-2993, October 2014.

[12] J. Ahn and B. K. Lee, "High-efficiency adaptive-current charging strategy for electric vehicles considering variation of internal resistance of lithium-ion battery," IEEE Trans. Power Electron. vol. 34, pp. 3041-3052, June 2018.

[13] Y. Liu and Y. Luo, "Search for an optimal rapid-charging pattern for li-ion batteries using the taguchi approach," IEEE Trans. Ind. Electron. vol. 57, pp. 3963-3971, November 2009.

[14] Y. Wang, Y. Li, L. Jiang, Y. Huang, and Y. Cao, "Pso-based optimization for constant-current charging pattern for li-ion battery," Chin. J. Electr. Eng. vol. 5, pp. 72-78, August 2019.

[15] J. Jiang, Q. Liu, C. Zhang, and W. Zhang, "Evaluation of acceptable charging current of power li-ion batteries based on polarization characteristics," IEEE Trans. Ind. Electron. vol. 61, pp. 6844-6851, April 2014.

[16] H. Bai, Z. Zhao, and C. Mi, "Framework and research methodology of short-timescale pulsed power phenomena in high-voltage and high-power converters," IEEE Trans. Ind. Electron. vol. 56, pp. 805-816, August 2008.

[17] Y. Liu, X. Zhu, Z. Mao, J. Kang, and J. Shen, "Loss analysis of gan-based dual active bridge converter for power electronic transformer," 2020 IEEE 9th International Power Electronics and Motion Control Conference (IPEMC2020-ECCE Asia). pp. 2390-2395, December 2020.

[18] F. Yazdani, S. Haghbin, T. Thiringer, and M. Zolghadri, "Accurate power loss calculation of a three-phase dual active bridge converter for zvs and hard-switching operations," 2017 IEEE Vehicle Power and Propulsion Conference (VPPC). pp. 1-5, December 2017.